Towards Explainable Deep Learning in Oncology: Integrating EfficientNet-B7 with XAI techniques for Acute Lymphoblastic Leukaemia

Dost Muhammad[1,†], Ayse Keles[2] and Malika Bendechache[1]

[1]*ADAPT Centre, School of Computer Science, University of Galway, Ireland*

[2]*Ankara Medipol University, Türkiye*

Abstract

Acute Lymphoblastic Leukaemia (ALL), presents a potential risk to human health due to its rapid progression and impact on the body's blood-producing system. The accurate diagnosis derived through investigations plays a crucial role in formulating effective treatment plans that can influence the likelihood of patient recovery. In the pursuit of improving diagnostic accuracy, diverse Machine Learning (ML) and Deep Learning (DL) approaches have been employed, demonstrating significant improvement in analyzing intricate biomedical data for identifying ALL. However, the complex nature of these algorithms often makes them difficult to comprehend, posing challenges for patients, medical professionals, and the wider community. To address this issue, it is essential to clarify the functioning of these ML/DL models, strengthen trust and providing users with a clearer understanding of diagnostic outcomes. This paper introduces an innovative framework for ALL diagnosis by incorporating the EfficientNet-B7 architecture with Explainable Artificial Intelligence (XAI) methods. Firstly, the proposed model accurately classified the ALL utilizing C-NMC-19 and Taleqani Hospital datasets. The efficacy of the proposed model was rigorously validated utilizing established evaluation metrics notably AUC, mAP, Accuracy, Precision, Recall, and F1-score. Secondly, the XAI approaches namely, Grad-CAM, LIME and IG were applied to explain the proposed model decision. Our contributions on pioneering the explanation of EfficientNet-B7 decisions using XAI for the diagnosis of ALL, set a new benchmark for trust and transparency in the medical field.

Keywords

XAI for Healthcare, eXplainble medical imaging, Leukemia diagnosis, EfficientNet-B7

1. Introduction

The hematological composition of humans is primarily comprised of erythrocytes (Red blood cells, or RBCs), with leukocytes (White blood cells, or WBCs) and thrombocytes (platelets) also playing crucial roles. These components are indispensable for transporting vital substances throughout the body [1]. Thrombocytes are crucial in the clotting mechanism, erythrocytes are essential in conveying oxygen, and white blood cells (WBCs) are essential for infection prevention and defence. Variations in the WBC count can have a substantial impact on the human immune system, although it accounts for only 1% of the blood volume, highlighting the diagnostic and therapeutic significance of blood [2].

Leukaemia is categorised as an oncological condition and epitomises a significant threat within the broad spectrum of life-threatening pathologies afflicting humans. This is particularly noticeable when WBCs proliferate abnormally and uncontrolled, this malady disrupts normal hematopoietic function [3]. In the light of projections by the World Health Organization, a significant rise of nearly 50% in cancer incidence and death rates is expected by 2040 [1]. Thus, there is an urgent need for advances in detection techniques and diagnosis of this disease [4].

Microscopic differentiation between leukaemia and normal cells presents significant challenges, that are made more difficult by technical problems including illumination mistakes and staining noise [5]. These obstacles make it difficult to accurately characterize the cellular traits that are essential for a leukaemia diagnosis, particularly acute lymphoblastic leukaemia (ALL), which is notorious for its aggressive progression and its impact on haematopoiesis within bone marrow [6]. Traditional diagnostic approaches, despite their utility, suffer from being invasive, time-intensive and prone to diagnostic inaccuracies. The advent of medical imaging technology and computational have provided a non-invasive alternative; however, radiologists' manual review of large image datasets is time-consuming, error-prone, and ineffective for the subtle differences needed for leukaemia diagnosis.

DL-based approaches have been widely applied in the extant literature for the identification and classification of ALL. As illustrated by Abir [7], Mondal [4], Amin [8], and Kasani [9], scholarly investigations have explored many DL models, including VGG19, ResNetV2, Inception-ResNetV2, DenseNet-121, Xception, MobileNet, VGG-16, and EfficientNet-B3, as well as general frameworks like CNN and DNN. These studies have used extremely detailed evaluation metrics to ascertain the efficiency of their models. However, a noticeable gap exists in explaining the effectiveness and operation of these models [10]. In particular, patients, healthcare providers, and the general public may encounter difficulties in grasping the nuanced outcomes, which could undermine their confidence in the judgements made by DL models. Consequently, it is imperative to demystify the particular components and features that drive the decision-making process of these DL models. This initiative aimed to enhance the understanding level of patients, medical practitioners and the wider community to grasp the inner workings of DL models. Thereby, it can promote a deeper comprehension, confidence and trust in these cutting-edge technologies. It paves the way for incorporating the interpretability of these models into Clinical Decision Support Systems (CDSS) and bringing technological advancements in line with their useful applications in healthcare.

In response to the critical need for advanced diagnostic approaches in the battle against Acute Lymphoblastic Leukaemia (ALL) [11], our work employs the sophisticated EfficientNet-B7 [12], an Avant-grade CNN framework. This model is fine-tuned to accurately identify and classify white cells in the microscopic image as either ALL or normal. To reconcile the EfficientNet-B7's high performance with explainability, we integrated Explainable Artificial Intelligence (XAI) techniques such as Local interpretable model explanation (LIME)[13], Gradient-weighted class activation map (Grad-CAM) [14] and Integrated Gradients (IG)[15]. The XAI approaches provide elucidation on the model's decision-making pathway, enriching the explainability of the diagnostic process for medical professionals and patients, thereby increasing trust and ensuring

---

[1]https://platform.who.int/mortality/themes/theme-details/topics/indicator-groups/indicator-group-details/MDB/leukaemia

diagnostic veracity. This paper is structured as follows: a review of the extant literature is found in Section 2, Section 3 outlines the methodology employed, Section 4 represents the discussion/results and Section 5 concludes the paper with an overview of future research.

2. Relveant Studies

In the arena of current research, this study explored a myriad of architectural methodologies, evaluation criteria and explanations: the employment of EfficientNet-B7 with the integration of XAI stands as a novel contribution. In the extant literature, various CNN-based approaches presented in Table 1 such as VGG-16/19, Inception-V3, ResNetV2/50, DenseNet121, EfficientNet-B3 and aggregation-based were applied. The choice of EfficientNet-B7 is strategic and is distinguished by its balance scaling offering a potent combination of accuracy and efficiency. In contrast to focusing only on established evaluation metrics, this work utilized comprehensive metrics namely AUC and mAP as well for providing the granular and nuanced analysis of the model performance. Moreover, the utilization of the C-NMC-19 dataset aligns this study with the available implementations for an immediate comparison of findings. Additionally, we employed another dataset, namely the Taleqani Hospital dataset, in our experimental work, and our proposed model demonstrated remarkable performance on this dataset as well. In stark contrast to the broader field, this study distinguishes itself from the prevailing trends by weaving in XAI, an aspect frequently neglected by others. The integration of Grad-CAM, LIME and IG with EfficientNet-B7 showcased additional clarity and explanation of the model's decision. The existing literature shows limited examples of XAI, with notable Abir et.al [7] and Uysal et.al [16] who used LIME and SHAP. Therefore, this study not only pushes the boundaries of evaluation and validation but also acts as a pioneer in the sphere of XAI, potentially setting a new standard for future research in Leukaemia.

Table 1
Comparison with Extant Literature

Researchers	Architecture	Perf-Metrics	Dataset	Integration with XAI
Mondal et al.[4]	VGG-16, InceptionResNet-V2, MobileNet, DenseNet-121	Accuracy, AUC	C-NMC-19	No
Amin et al.[8]	ECA-Net utilizing VGG-16	Accuracy, Sensitivity, Specificity	C-NMC-19	No
Khandekar et al.[17]	Res-Net50, Resnext-50, VGG-16, YOLOv4	mAP, Recall, F1-score	C-NMC-19	No
Kasani et al.[9]	Aggregation-based architecture of VGG19 and NASNetLarge	Accuracy, Precision, Recall, F1-score	ISBI-19	No
El-ghani et al.[18]	EfficientNetB3	Accuracy, Precision, Recall, F1-score	C-NMC-19	No
Ying et al.[19]	Deep Ensemble Learning	F1-score	ISBI-19	No
Jiang et al.	ViT-CNN	Accuracy, Precision	ISBI-19	No
Abir et al.[7]	Inception-V3	Accuracy, F1-score	ISBI-19	LIME
Uysal et al.[16]	Decision Tree Regressor	Accuracy, F1-score	ChEMBL version	SHAP
Proposed work	EfficientNet-B7	Accuracy, Precision, Recall, F1-score, AUC, mAP	C-NMC-19, Taleqani Hospital	Grad-CAM, LIME, IG
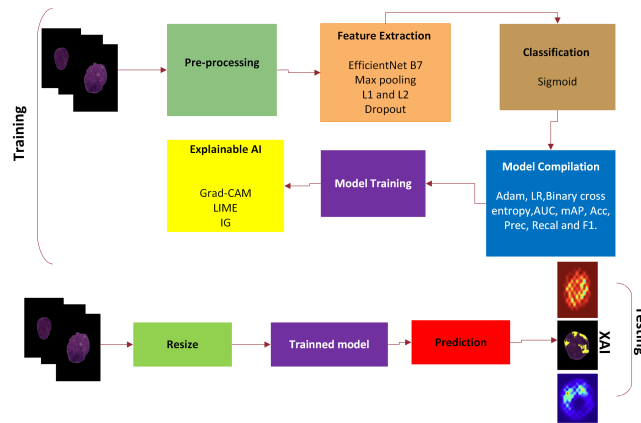
Figure 1: Workflow of the Proposed Methodology.

3. Methodology

The proposed workflow is illustrated in Figure 1, highlighting the key steps in the training and testing phases. In the training phase, the workflow comprises pre-processing, feature extraction and model training, while in the testing, the workflow transitions from image resizing to model prediction and concludes with XAI approaches.

3.1. Description of Datasets

Our study utilized two different datasets. Firstly, a refined dataset [20] that contains either cancerous or normal cells derived from real-world microscopic images, comprising 60% ALL and 40% Normal images. Noise and illumination errors in the images were corrected using an stain colour normalization technique [21]. The ground truth provided by the expert oncologist underpins the reliability of the dataset for validating the computational models. The second dataset considered in this study was prepared at the bone marrow laboratory of Taleqani Hospital in Tehran [22]. It comprises 3,256 peripheral blood smear (PBS) images from 89 patients suspected of having ALL; the dataset is imbalanced. These images were meticulously prepared and stained by skilled laboratory staff. The datasets were divided into two parts: training images (75%) and testing images (25%), used to ensure a sufficient amount of data for both training and testing purposes.

3.2. Preprocessing

In the pre-processing stage, the considered datasets underwent a systematic filtration based on image file extension pinpointing PNG, JPG, JPEG and GIF. After the previous step, the dataset was divided into two subsets training and testing. A necessary adjustment to ensure compatibility aligns with the input requirement of the CNN [23], the images were uniformly scaled to a dimension of 224x224 in the final phase.

3.3. EfficientNetB7

In this study, we carefully selected the methods and hyperparameters based on a combination of empirical methods and established best practices to optimize performance. We used the EfficientNet-B7 base model [12], trained on the Image-Net dataset was utilized via the Keras framework. The baseline model was able to utilize the pre-trained weights using the features of Image-Net and to instantly improve the performance of image recognition. EfficientNet-B7 is a CNN with feed-forward training that starts from the input layer to the classification layer illustrated in Eq. 1. Backpropagation error starts at the classification phase to the starting input layer as one pass is complete. As described by Eq. 1, information is passed from neuron q of $(l-1)$th to the neuron p of the lth layer, where W_{pq}^l is the connections' weight between the two neurons within the lth layer [24].

$$I_p^l = \sum_{q=1}^{n} W_{pq}^l a_p + \text{bias}_p \tag{1}$$

The base model was configured without the top layer specifically tailored to our task requirements, allowing for a customized output layer. In order to facilitate feature map reduction and abstraction, we applied maximal pooling after the base model output. Maximal pooling significantly enhanced the most silent features through spatial down-sampling, which not only reduced the computational load but also ensured robustness to variations in input images. After the initial output, batch normalization were employed, to normalized the inputs for subsequent layers using adjustment and activation scaling. Following this, a dense layer was integrated with L1 and L2 regularization [25] illustrated in Eq. 2 to curtail the overfitting. The regularization parameters were selected precisely to find balance between the model complexity and the fidelity of the training data.

$$L1(\theta) = \lambda \sum_{i=1}^{n} |\theta_i| \quad \bigg| \quad L2(\theta) = \lambda \sum_{i=1}^{n} |\theta_i|^2 \tag{2}$$

Where θ represent weights, n is number of parameters in the model and the regularization strength is λ. The integration of mentioned techniques batch normalization, regularization and then the utilization of dropout [26] illustrated in Eq. 3: effectively fine-tuned the balance between reducing overfitting and maintaining the complexity and integrity of the model aligning closely with the unique aspect of the training dataset.

$$x_j^{(l)} = r_j^{(l)} \cdot f\left(x_j^{(l)}\right) \tag{3}$$

Where, j denotes a neuron within the layer lth which employs activation function f. Here, $r_j^{(l)}$ is a random variable, input is $x_j^{(l)}$ and $\hat{x}_j^{(l)}$ represents the output of this neuron. The EfficientNet-B7 concludes with an output layer that integrated dense layer with a sigmoid activation function for classification. In the model compilation phase, the Adamax optimizer is applied due to its proven effectiveness, especially in dealing embeddings and enhancing the model optimization process [27].

3.4. Explainability

EfficientNet-B7 with its complex architecture extracts intricate features from the input cancerous images essential for high accuracy in ALL identification and classification. However, due to the deep architecture of this model, understanding the decision process for the Non-Tech community is challenging. In response to this gap, we employed XAI approaches namely Local Interpretable Model-agnostic Explanation (LIME) [28], Gradient-weighted Class Activation Mapping (Grad-CAM) [29], and Integrated Gradients (IG) [15] to provide the visual explanation and interpretation of the image features which are influencing the model's prediction. Grad-CAM utilises the gradients of the last convolutional layer (top_activation) to generate a heatmap illustrated in Eq. 4 that illuminates the critical region within the image which affects the model decision.

$$L_{GC}^c = \text{ReLU}\left(\sum_k \alpha_k^c \cdot f^k\right) \tag{4}$$

The Eq. 4 represents this localization map for class c, where L_{GC}^c highlights important regions, ReLU ensures non-negative output, α_k^c indicates the importance of feature map f^k for class c, and f^k are the feature maps from convolutional layers.

LIME provides an explanation by perturbing the input images, observing the changes in the model prediction, and pinpointing the image features that substantially impact the model's prediction as shown in Eq. 5 [30].

$$L(f, g, \pi_x) + \Omega(g) = \sum_{i=1}^{N} w_i \cdot \left(f(x_i') - g(x_i')\right)^2 + \Omega(g) \tag{5}$$

In Eq. 5, $L(f, g, \pi_x)$ measures the difference between the original model f and the interpretable model g, with π_x as the proximity measure. Weights w_i are for perturbed samples x_i'. $\Omega(g)$ is the complexity penalty for g.

IG is an XAI approach that offers a way to attribute the prediction of the model to its input features, notably pixels for images by integrating the output gradients from a baseline to the actual image; thereby highlighting the role of an individual pixel in image analysis as shown in Eq. 6.

$$IG_i(x) = (x_i - x_i') \times \int_{\alpha=0}^{1} \left(\frac{\partial f(x' + \alpha \times (x - x'))}{\partial x_i}\right) d\alpha \tag{6}$$

.

Here, $IG_i(x)$ is the integrated gradient for feature i, x_i is the actual input, x_i' is the baseline input, and α scales the difference between inputs.

4. Results and Discussion

In this study, we employed the EfficientNet-B7, a forefront CNN architecture for the vital task of identification and classification of ALL utilizing the microscopic images. Following the model's training and validation phase, we integrated the XAI methodologies to demystify and explain the model's prediction decision.

4.1. Classification

The EfficientNet-B7 exhibited remarkable performance presented in Table 2 across all considered metrics. The proposed model demonstrated its high level of reliability in accurately detecting ALL, achieving an accuracy of 97.13% on the C-NMC-19 dataset and 96.78% on the Taleqani Hospital dataset. The precision metric recorded at 99.32% for C-NMC-19 dataset and 97.00% for Taleqani Hospital dataset , the model proves its adeptness at significantly reducing the false positive, which is crucial in diagnosis to avoid unnecessary anxiety and medical intervention for patients. The recall score of 92.42% and 96.25% on C-NMC-19 dataset and Taleqani Hospital dataset respectively, indicates its strength in identifying the vast majority of genuine ALL cases, ensuring minimal missed diagnosis.

Table 2
EfficientNet-B7 classification performance scores on all datasets.

| Dataset	Accuracy%	Precision%	Recall%	F1-score%	AUC%	mAP%
C-NMC-19	97.13	99.32	92.42	95.75	96.04	94.45
Taleqani Hospital	96.78	97.00	96.25	96.57	99.85	99.56

Furthermore, the F1-scores of 95.75% on C-NMC-19 dataset and 96.57% on Taleqani Hospital dataset , demonstrated the robust and harmonious balance between the recall and precision. Additionally, the AUC score of 96.04% on C-NMC-19 dataset and 99.85% on Taleqani Hospital dataset highlights the superior performance of the model in distinguishing between ALL and healthy classes accurately. Furthermore, the last evaluation metric mAP scores according to Table 2 are 94.45% on C-NMC-19 dataset and 99.56% on Taleqani Hospital dataset, emphasising the model's consistent and reliable performance across different threshold levels.

4.2. Explanation

XAI approaches namely LIME, Grad-CAM and IG were applied to the classification model to explain the predictive decision and enhance the trust of medical professionals and patients. Comparative visualization with the original image of the mentioned techniques is illustrated in Fig 2 and 3.

The Grad-CAM generated heatmaps in Fig 2(B) and Fig 3 (F), which offered a visual representation of the areas within the original ALL image that contribute most to the model's prediction. The process involves the extraction of gradient values from the last convolutional layer (top_actovation) concerning ALL cancer, which indicates the non-functional white cells in the Leukaemia imagery. According to heatmap (B) in Fig 2, the red area indicates the highest contribution, whereas the areas in blue contribute the least. Similarly, the heatmap (F) shown in the Fig 3 illustrates that the areas marked in white are the highest contributors to the model's decision making process, whereas areas in other colors contribute less significantly.

In the LIME explanation Fig 2 (C) and Fig 3 (G), the yellow areas are identified as key influencers in steering the model's decision. LIME provided an explanation based on the perturbation of the input ALL image and observed the effect on the output.LIME was initially utilized to explain the Inception-V3 by[7]; however, it has shown enhanced effectiveness with
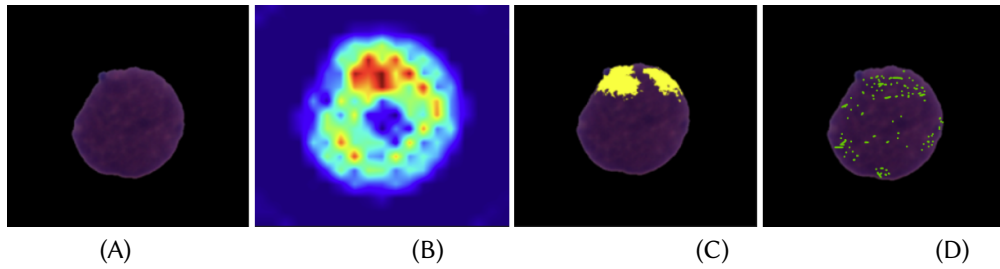
Figure 2: Comprehensive Visualization of XAI Techniques on C-NMC-19 dataset: (A) Original Image, (B) Grad-CAM, (C) LIME and (D) IG.
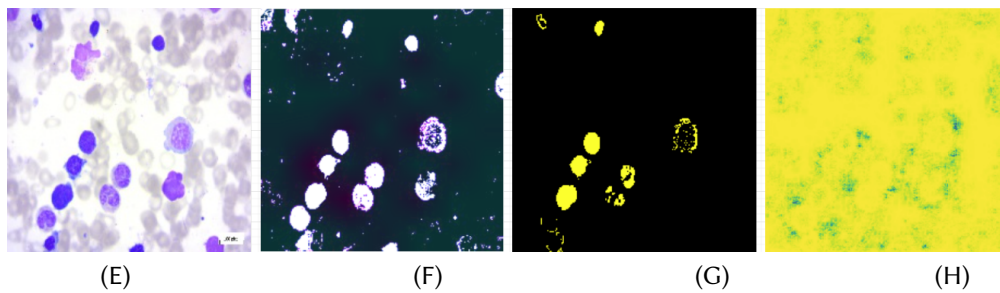
Figure 3: Comprehensive Visualization of XAI Techniques on Taleqani Hospital dataset: (A) Original Image, (B) Grad-CAM, (C) LIME and (D) IG.

the EfficientNet-B7. In Fig 2 (D) and Fig 3 (H), the regions highlighted in green represent positive contributions to the model, as determined by the IG method.

Conclusively, the Grad-CAM offered more precise localization of influential regions as compared to LIME and IG, often better for the identification and detection of un-functional white cells in the microscopic image.

5. Conclusion and Future research directions

In this study, we have effectively presented the integration of EfficientNet-B7 with Explainable AI methods on two different datasets (C-NMC-19 and Taleqani Hospital) to improve the diagnosis process and explain the model's decision through Grad-CAM, LIME and IG for ALL. The incorporation of comprehensive evaluation metrics namely AUC , mAP, Accuracy, Precision, Recall and F1-score further validated the efficacy and reliability of our proposed framework presented in Table 2, setting a new phase for AI-driven diagnostic in oncology.

Conclusively, this work not only proposed a novel framework for the diagnosis of ALL but also set a new trend for the future of AI in medicine, balancing the scales between computational innovation and the imperative for explainability, clarity and trust in medical diagnostics. In future, we aim to implement different architectures and XAI approaches to extend this framework to diverse haematological diseases for enhancing the diagnostic process.

Acknowledgement

References

[1] A. H. Mageed, S. A. Faraj, M. I. Maleek, et al., A comparative study of hematological and biochemical parameters in leukemia patients and healthy persons, HIV Nursing 23 (2023) 1599–1602.

[2] M. Zolfaghari, H. Sajedi, A survey on automated detection and classification of acute leukemia and wbcs in microscopic blood cells, Multimedia Tools and Applications 81 (2022) 6723–6753.

[3] A. M. Gocher, C. J. Workman, D. A. Vignali, Interferon-γ: teammate or opponent in the tumour microenvironment?, Nature Reviews Immunology 22 (2022) 158–172.

[4] C. Mondal, M. K. Hasan, M. Ahmad, M. A. Awal, M. T. Jawad, A. Dutta, M. R. Islam, M. A. Moni, Ensemble of convolutional neural networks to diagnose acute lymphoblastic leukemia from microscopic images, Informatics in Medicine Unlocked 27 (2021) 100794.

[5] M. Ghaderzadeh, M. Aria, A. Hosseini, F. Asadi, D. Bashash, H. Abolghasemi, A fast and efficient cnn model for b-all diagnosis and its subtypes classification using peripheral blood smear images, International Journal of Intelligent Systems 37 (2022) 5113–5133.

[6] B. G. Raphael, Normal blood cells are produced in the bone marrow. a, Medical Aspects of Disability: A Handbook for the Rehabilitation Professional (2005) 325.

[7] W. H. Abir, M. F. Uddin, F. R. Khanam, T. Tazin, M. M. Khan, M. Masud, S. Aljahdali, et al., Explainable ai in diagnosing and anticipating leukemia using transfer learning method, Computational Intelligence and Neuroscience 2022 (2022).

[8] M. M. Amin, S. Kermani, A. Talebi, M. G. Oghli, Recognition of acute lymphoblastic leukemia cells in microscopic images using k-means clustering and support vector machine classifier, Journal of medical signals and sensors 5 (2015) 49.

[9] P. H. Kasani, S.-W. Park, J.-W. Jang, An aggregated-based deep learning method for leukemic b-lymphoblast classification, Diagnostics 10 (2020) 1064.

[10] S. Nasir, R. A. Khan, S. Bai, Ethical framework for harnessing the power of ai in healthcare and beyond, arXiv preprint arXiv:2309.00064 (2023).

[11] A. Redaelli, B. Laskin, J. Stephens, M. Botteman, C. Pashos, A systematic literature review of the clinical and epidemiological burden of acute lymphoblastic leukaemia (all), European journal of cancer care 14 (2005) 53–62.

[12] M. Tan, Q. Le, EfficientNet: Rethinking model scaling for convolutional neural networks, in: K. Chaudhuri, R. Salakhutdinov (Eds.), Proceedings of the 36th International Conference on Machine Learning, volume 97 of *Proceedings of Machine Learning Research*, PMLR, 2019, pp. 6105–6114. URL: https://proceedings.mlr.press/v97/tan19a.html.

[13] J. Shin, Feasibility of local interpretable model-agnostic explanations (lime) algorithm as an effective and interpretable feature selection method: comparative fnirs study, Biomedical Engineering Letters (2023) 1–15.

[14] E. Kellener, I. Nath, A. Ngo, T. Nguyen, J. Schuman, C. Adler, A. Kartikeya, Utilizing segment anything model for assessing localization of grad-cam in medical imaging, arXiv preprint arXiv:2306.15692 (2023).

[15] M. Sundararajan, A. Taly, Q. Yan, Axiomatic attribution for deep networks, in: International conference on machine learning, PMLR, 2017, pp. 3319–3328.

[16] I. Uysal, U. Kose, Development of a simulation environment for the importance of histone

deacetylase in childhood acute leukemia with explainable artificial intelligence, BRAIN. Broad Research in Artificial Intelligence and Neuroscience 14 (2023) 254–286.

[17] R. Khandekar, P. Shastry, S. Jaishankar, O. Faust, N. Sampathila, Automated blast cell detection for acute lymphoblastic leukemia diagnosis, Biomedical Signal Processing and Control 68 (2021) 102690.

[18] S. Abd El-Ghany, M. Elmogy, A. A. El-Aziz, Computer-aided diagnosis system for blood diseases using efficientnet-b3 based on a dynamic learning algorithm, Diagnostics 13 (2023) 404.

[19] Y. Liu, F. Long, Acute lymphoblastic leukemia cells image analysis with deep bagging ensemble learning, in: ISBI 2019 C-NMC Challenge: Classification in Cancer Cell Imaging: Select Proceedings, Springer, 2019, pp. 113–121.

[20] S. Mourya, S. Kant, P. Kumar, A. Gupta, R. Gupta, ALL Challenge dataset of ISBI 2019 (C-NMC 2019), The Cancer Imaging Archive, 2019. doi:10.7937/tcia.2019.dc64i46r, https://doi.org/10.7937/tcia.2019.dc64i46r.

[21] M. Dabass, J. Dabass, S. Vashisth, R. Vig, A hybrid u-net model with attention and advanced convolutional learning modules for simultaneous gland segmentation and cancer grade prediction in colorectal histopathological images, Intelligence-Based Medicine 7 (2023) 100094.

[22] M. Aria, M. Ghaderzadeh, D. Bashash, H. Abolghasemi, F. Asadi, A. Hosseini, Acute lymphoblastic leukemia (all) image dataset, https://www.kaggle.com, 2021. doi:10.34740/KAGGLE/DSV/2175623.

[23] L. F. Brillet, Convolutional Neural Networks for embedded vision, Ph.D. thesis, Université Grenoble Alpes [2020-....], 2020.

[24] A. Ghosh, B. Soni, U. Baruah, Transfer learning-based deep feature extraction framework using fine-tuned efficientnet b7 for multiclass brain tumor classification, Arabian Journal for Science and Engineering (2023) 1–22.

[25] M. A. Albahar, M. Binsawad, Deep autoencoders and feedforward networks based on a new regularization for anomaly detection, Security and Communication Networks 2020 (2020) 1–9.

[26] D. Muhammad, I. Ahmad, M. I. Khalil, W. Khalil, M. O. Ahmad, A generalized deep learning approach to seismic activity prediction, Applied Sciences 13 (2023) 1598.

[27] T. Chauhan, H. Palivela, S. Tiwari, Optimization and fine-tuning of densenet model for classification of covid-19 cases in medical imaging, International Journal of Information Management Data Insights 1 (2021) 100020.

[28] T. Vermeire, D. Brughmans, S. Goethals, R. M. B. de Oliveira, D. Martens, Explainable image classification with evidence counterfactual, Pattern Analysis and Applications 25 (2022) 315–335.

[29] Y. Zhang, D. Hong, D. McClement, O. Oladosu, G. Pridham, G. Slaney, Grad-cam helps interpret the deep learning models trained to classify multiple sclerosis types using clinical brain magnetic resonance imaging, Journal of Neuroscience Methods 353 (2021) 109098.

[30] A. Bhattacharya, Applied Machine Learning Explainability Techniques: Make ML models explainable and trustworthy for practical applications using LIME, SHAP, and more, Packt Publishing Ltd, 2022.